Research article

A uniform LMI formulation for tuning PID, multi-term fractional-order PID, and Tilt-Integral-Derivative (TID) for integer and fractional-order processes

Farshad Merrikh-Bayat

Department of Electrical and Computer Engineering, University of Zanjan, Zanjan, Iran

ABSTRACT

In this paper first the Multi-term Fractional-Order PID (MFOPID) whose transfer function is equal to $\sum_{j=1}^{N} k_j s^{\alpha_j}$, where k_j and α_j are unknown and known real parameters respectively, is introduced. Without any loss of generality, a special form of MFOPID with transfer function $k_p + k_i/s + k_{d1}s + k_{d2}s^\mu$ where k_p, k_i, k_{d1}, and k_{d2} are unknown real and μ is a known positive real parameter, is considered. Similar to PID and TID, MFOPID is also linear in its parameters which makes it possible to study all of them in a same framework. Tuning the parameters of PID, TID, and MFOPID based on loop shaping using Linear Matrix Inequalities (LMIs) is discussed. For this purpose separate LMIs for closed-loop stability (of sufficient type) and adjusting different aspects of the open-loop frequency response are developed. The proposed LMIs for stability are obtained based on the Nyquist stability theorem and can be applied to both integer and fractional-order (not necessarily commensurate) processes which are either stable or have one unstable pole. Numerical simulations show that the performance of the four-variable MFOPID can compete the trivial five-variable FOPID and often excels PID and TID.

© 2017 ISA. Published by Elsevier Ltd. All rights reserved.

1. Introduction

Fractional-order PID (FOPID) was introduced in 1999 by Podlubny as a generalization of trivial PID controllers [1]. The transfer function of the ideal FOPID, also known as $PI^\lambda D^\mu$, is defined as [1]:

$$C_{FOPID}(s) = k_p + \frac{k_i}{s^\lambda} + k_d s^\mu, \tag{1}$$

where k_p, k_i, $k_d \in \mathbb{R}$ and λ, $\mu \in \mathbb{R}^+$ are unknown parameters of controller to be tuned. See, for example, [2] for the possible time-domain interpretations of the fractional powers of s in (1) and their properties. Considering the fact that FOPID has five parameters to tune, two more than the classical PID, it is expected that it leads to a higher performance compared to PID especially in dealing with problems with complicated control objectives [3]. Various successful applications of FOPID controllers have been reported in the literature. Some examples are motion control [4], unmanned aerial vehicle [5], path tracking control of tractors [6], and control of a solar furnace [7]. FOPID controllers can be realized using either analogue [8,9] or digital techniques [10,11].

Another fractional-order controller which is closely related to FOPID and discussed in this paper is the Tilt-Integral-Derivative (TID). The transfer function of TID is defined as [12]:

$$C_{TID}(s) = \frac{k_t}{s^{1/n}} + \frac{k_i}{s} + k_d s, \tag{2}$$

where again k_t, k_i, and k_d are unknown real parameters to be calculated, and n is an unknown positive integer often considered equal to 2 or 3 before tuning other parameters [12]. Some properties of TID have been studied in [13]. A method for tuning its parameters is also presented therein.

So far, a wide variety of techniques have been proposed for tuning the parameters of FOPID. For example, tuning the parameters based on open-loop shaping [14,3], Bode's ideal transfer function [15,16], minimization of performance indices like ISE and IAE [17,18], optimization of load disturbance subject to a constraint on the maximum sensitivity (M_s) [19], simultaneous adjustment of phase and gain margin to the desired values [20], and fractional-order root-locus method [21] can be found in the literature. Some of these methods like those presented in [17] and [18] lead to explicit tuning rules which can be applied to first-order plus time delay (FOPTD) or integrator plus dead time (IPDT) or unstable first-order plus dead-time (UFOPDT) processes. It is worth mentioning that almost all of the methods developed so far for tuning FOPID controllers are based on solving a kind of optimization problem. Some researchers have used meta-heuristic optimization algorithms for solving such problems; see for example [22–24].

During the past decades many control problems have been successfully formulated as convex optimization problems

E-mail address: f.bayat@znu.ac.ir

involving Linear Matrix Inequalities (LMIs) [25]. Recently, some researchers have applied LMIs for stability analysis and controller synthesis for fractional-order systems (FOS). For example, LMI approach for stability analysis of a system governed by the state-space equation $D^\nu x(t) = Ax(t)$ where D^ν is a fractional-order derivative operator, $A \in \mathbb{R}^{n \times n}$, $x(t) \in \mathbb{R}^n$ and $0 < \nu < 2$ is presented in [26]. LMI-based sufficient conditions for robust stability and stabilization of linear time-invariant FOS are presented in [27]. In the field of synthesis of control laws, pseudo-state feedback stabilization of commensurate FOS [28] and H_∞ output feedback control of commensurate FOS [29], both using LMIs, are reported in the literature. LMIs for calculating the bounds on the norms of FOS are presented in [30].

The aim of this paper is to propose a method for tuning a kind of FOPID using LMIs. For this purpose first a new fractional-order controller which is defined by adding a fractional differentiator of fixed order to the classical PID, is introduced. Then LMIs for shaping the open-loop frequency response when the proposed controller is applied are developed. The proposed approach makes it possible to use advantages of convex optimization and fractional-order operators to solve a control problem.

The rest of this paper is organized as the following. The main results including the proposed structure for fractional-order controller and the corresponding LMIs for open-loop shaping are presented in Section 2. Four illustrative examples are presented in Section 3, and Section 4 concludes the paper.

2. Multi-term FOPID: definition and tuning

In this section first the multi-term FOPID (MFOPID) is introduced. Then separate LMIs for closed-loop stability (of sufficient type), adjustment of phase margin (PM), adjustment of only the open-loop phase, and adjustment of only the open-loop gain are presented. In practice, the user can apply the LMIs for stability in combination with any of the other LMIs to design the controller by loop shaping. At the end of this section another approach for controller design which is also based on LMIs and applicable to higher order and time-delayed processes with one unstable pole is presented.

2.1. The proposed multi-term FOPID

Before introducing the MFOPID controller first note that unlike FOPID, PID and TID (assuming a fixed value for n in (2)) are linear in their parameters. More precisely, considering the vector of unknown parameters as

$$X = \begin{bmatrix} k_p\, k_i\, k_d \end{bmatrix}^T, \tag{3}$$

the classical ideal PID can be expressed as

$$C_{PID}(s) = k_p + \frac{k_i}{s} + k_d s = \begin{bmatrix} 1\ s^{-1} s \end{bmatrix} X = W_{PID}(s)X, \tag{4}$$

which is linear in X. Similarly, assuming

$$X = \begin{bmatrix} k_t\, k_i\, k_d \end{bmatrix}^T, \tag{5}$$

the TID defined in (2) can be expressed as

$$C_{TID}(s) = \begin{bmatrix} s^{-1/n} s^{-1} s \end{bmatrix} X = W_{TID}(s)X, \tag{6}$$

which again assuming a certain value for n is linear in X. But the FOPID given in (1) cannot be expressed in the same way unless the values of λ and μ are assumed to be fixed in advance. The possibility of writing a controller with transfer function $C(s)$ in the form of $C(s) = W(s)X$, where $W(s)$ and X are the known *weights* and the

unknown *parameters* vectors, respectively, is an advantage since it makes it possible to calculate X through LMIs and convex optimization algorithms as it will be discussed in the following. The above discussion motivates us to present a new definition for FOPID controller which is firstly linear in the vector of tuning parameters, and secondly, has more tuning parameters compared to PID and can mimic the performance of traditional FOPID defined in (1).

According to the above discussion the transfer function of MFOPID is defined as

$$C_{MFOPID}(s) \triangleq \sum_{j=1}^{N} k_j s^{\alpha_j} = \begin{bmatrix} s^{\alpha_1} s^{\alpha_2} \ldots s^{\alpha_N} \end{bmatrix} X = W_{MFOPID}(s)X, \tag{7}$$

where $\alpha_1, \ldots, \alpha_N$ are known real constants, and

$$X = \begin{bmatrix} k_1 \ldots k_N \end{bmatrix}^T, \tag{8}$$

is the vector of real unknown parameters, and

$$W_{MFOPID}(s) = \begin{bmatrix} s^{\alpha_1} s^{\alpha_2} \ldots s^{\alpha_N} \end{bmatrix}, \tag{9}$$

is the weights vector which is known at each frequency.

Without any loss of generality, a special form of (7) as given in (10) is used in the numerical examples of this paper:

$$C_{MFOPID}(s) = k_p + \frac{k_i}{s} + k_{d1}s + k_{d2}s^\mu, \tag{10}$$

where $0 < \mu < 2$ is a pre-determined positive real constant and the vector of unknown parameters is $X = \begin{bmatrix} k_p\, k_i\, k_{d1}\, k_{d2} \end{bmatrix}^T$. The controller in (10) can be though of as a PID accompanied with an extra fractional-order derivative operator. The reason for being interested in this controller is that the traditional integrator $1/s$ is sufficient for many applications while there is often a need for an extra phase lead which can be achieved by the term $k_{d2}s^\mu$ in (10). Note that in practice the order of integrator, λ, in (1) is often considered larger than or equal to unity since application of λ's smaller than unity leads to very slow convergence of the closed-loop step response to its final value, which is not desired. In the rest of this paper the transfer function of controller is considered as $C(s) = W(s)X$ for some $W(s)$ and X.

2.2. LMIs for closed-loop stability (stable process)

Consider the feedback system shown in Fig. 1 where here $P(s)$ is assumed to be stable. In this case it is concluded from the Nyquist stability theorem that the closed-loop system is also stable if and only if the Nyquist plot of $L(s) = C(s)P(s) = W(s)XP(s)$ does not encircle -1. Clearly, infinity many different Nyquist plots can be drawn which satisfy this condition. Fig. 2 shows a common approach to achieve closed-loop stability in this case where the Nyquist plot lies in the lower (upper) half-plane at all frequencies smaller (larger) than the phase crossover frequency, ω_{pc}, and at $\omega = \omega_{pc}$ we have $\text{Re}\{L(j\omega_{pc})\} > -1$ and $\text{Im}\{L(j\omega_{pc})\} = 0$. According to this figure the *sufficient* condition for closed-loop stability is the simultaneous satisfaction of (11)–(13):

$$\text{Im}\{L(j\omega)\} < 0, \ 0 \le \omega < \omega_{pc}, \tag{11}$$

$$\text{Re}\{L(j\omega_{pc})\} > -1 \quad \wedge \quad \text{Im}\{L(j\omega_{pc})\} = 0, \tag{12}$$
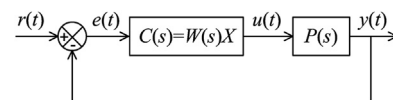
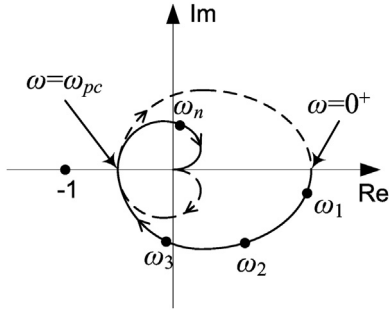

Fig. 1. The closed-loop system under consideration.

Fig. 2. Assuming that $P(s)$ is stable, the Nyquist plot of $L(s) = W(s)XP(s)$ must not encircle -1 for closed-loop stability.

$$Im\{L(j\omega)\} > 0, \quad \omega_{pc} < \omega. \tag{13}$$

Considering the fact that $W(j\omega)$ and $P(j\omega)$ can be decomposed to their real and imaginary parts as the following

$$W(j\omega) = W_r(j\omega) + jW_i(j\omega), \tag{14}$$

$$P(j\omega) = P_r(j\omega) + jP_i(j\omega), \tag{15}$$

substitution of (14) and (15) in $L(j\omega) = W(j\omega)XP(j\omega)$ yields

$$L(j\omega) = W_rXP_r - W_iXP_i + j(W_iXP_r + W_rXP_i). \tag{16}$$

Now substituting (16) in (11)–(13) results in the following four LMIs in X for closed-loop stability:

$$W_i(j\omega)XP_r(j\omega) + W_r(j\omega)XP_i(j\omega) < 0, \quad 0 \le \omega < \omega_{pc}, \tag{17}$$

$$W_r(j\omega_{pc})XP_r(j\omega_{pc}) - W_i(j\omega_{pc})XP_i(j\omega_{pc}) > -1, \tag{18}$$

$$-\epsilon < W_i(j\omega_{pc})XP_r(j\omega_{pc}) + W_r(j\omega_{pc})XP_i(j\omega_{pc}) < \epsilon, \tag{19}$$

$$W_i(j\omega)XP_r(j\omega) + W_r(j\omega)XP_i(j\omega) > 0, \quad \omega_{pc} < \omega. \tag{20}$$

Note that the equality constraint in (12) is written in the form of two inequality constrains in (19), where ϵ is a very small positive real constant, e.g. $\epsilon = 0.01$.

The main point about (17) and (20) is that these cannot be considered as LMIs in X unless ω is assumed to be known. Moreover, these two inequalities must be satisfied for all values of $0 \le \omega < \omega_{pc}$ and $\omega > \omega_{pc}$, respectively. To remove this difficulty, in practice it is sufficient to make sure that these two inequalities are satisfied only at certain frequencies like $\omega_1, ..., \omega_n$ as shown in Fig. 2. In other words, in practice the closed-loop stability can be formulated using (18) and (19) combined with sufficiently large number of LMIs in the form of (17) and (20) where each of them is evaluated at a different value of ω. Various simulations performed by author show that in dealing with many problems only a few sample frequencies, e.g. two or three, from each of the intervals $[0, \omega_{pc})$ and (ω_{pc}, ∞) is sufficient for this purpose (see the examples of Section 3 for more information). Note that ω_{pc} in (18) and (19) is an important design parameter since one can increase (decrease) it to arrive at a faster (slower) closed-loop system, until the limitations caused by non-minimum phase zeros, unstable poles, and time delays occur [31], ch. 5. Hence, in addition to satisfying the closed-loop stability, the designer can easily adjust the speed of closed-loop system through (17)–(20) by suitable choice of ω_{pc}.

There are some additional comments in relation to the stability LMIs given in (17)–(20). First, one can easily determine the desired lower bound for gain margin (GM) through (18). More precisely, in order to arrive at a closed-loop system with the minimum gain margin of $\overline{GM}$ ($\overline{GM} > 1$) the following linear constraint must be used instead of (18):

$$W_r(j\omega_{pc})XP_r(j\omega_{pc}) - W_i(j\omega_{pc})XP_i(j\omega_{pc}) > -1/\overline{GM}. \tag{21}$$

The second point is that application of (17)–(20) is limited to problems where the relative degree of open-loop system is at most equal to four. The reason is the results are obtained assuming that the Nyquist plot remains in the lower (upper) half-plane for $0 \le \omega < \omega_{pc}$ ($\omega_{pc} < \omega$), i.e., the maximum possible rotation of Nyquist plot is four quarters. Of course, this restriction is not serious in dealing with many real-world problems.

2.3. LMIs for closed-loop stability (process has one unstable pole)

Consider again Fig. 1 and assume that $P(s)$ has one unstable pole and its relative degree is at most equal to three, which means that its Nyquist plot can rotate at most three quarter planes as ω is increased from 0 to ∞. In this case according to the Nyquist stability theorem (assuming the standard clockwise contour) the closed-loop system is stable if and only if the Nyquist plot of $L(s)$ encircles the point -1 exactly once counterclockwise. Clearly, various scenarios with different degrees of conservativity can be imagined under which such an encirclement occurs. For example, this can be achieved by shaping $L(j\omega)$ such that its Nyquist plot remains in the upper half-plane for $0 \le \omega < \omega_{pc}$ and the lower half plane for $\omega_{pc} < \omega$ as shown in Fig. 3, where ω_{pc} is the desired phase crossover frequency. Using this scenario the sufficient condition for closed-loop stability is the simultaneous satisfaction of the conditions given in (22)–(24):

$$Im\{L(j\omega)\} > 0, \quad 0 \le \omega < \omega_{pc}, \tag{22}$$

$$Re\{L(j\omega_{pc})\} < -1 \quad \wedge \quad Im\{L(j\omega_{pc})\} = 0, \tag{23}$$

$$Im\{L(j\omega)\} < 0, \quad \omega_{pc} < \omega. \tag{24}$$

Now, for the given ω, substitution of $L(j\omega)$ from (16) in (22)–(24) yields the following LMIs in X:

$$W_i(j\omega)XP_r(j\omega) + W_r(j\omega)XP_i(j\omega) > 0, \quad 0 \le \omega < \omega_{pc}, \tag{25}$$

$$W_r(j\omega_{pc})XP_r(j\omega_{pc}) - W_i(j\omega_{pc})XP_i(j\omega_{pc}) < -1, \tag{26}$$
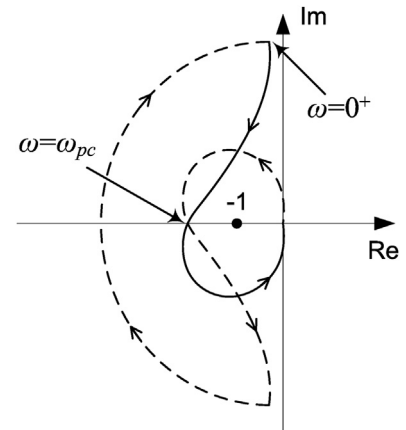

Fig. 3. Assuming that $P(s)$ has one unstable pole, the Nyquist plot of $L(s) = W(s)XP(s)$ must encircle -1 once counterclockwise for closed-loop stability.

$$-\epsilon < W_i(j\omega_{pc})XP_r(j\omega_{pc}) + W_r(j\omega_{pc})XP_i(j\omega_{pc}) < \epsilon, \tag{27}$$

$$W_i(j\omega)XP_r(j\omega) + W_r(j\omega)XP_i(j\omega) < 0, \quad \omega_{pc} < \omega, \tag{28}$$

where ϵ in (27) is a small positive real constant. Note that the equality constraint in (23) is written in the form of two inequality constraints in (27). One can also easily enter the desired value for the lower bound of GM to the stability LMIs presented in (25)–(28). For this purpose, in order to guarantee the closed-loop stability with the minimum GM of $\underline{GM}$ $(0 < \underline{GM} < 1)$ we can use (25), (27), and (28) in combination with (29) instead of (26):

$$W_r(j\omega_{pc})XP_r(j\omega_{pc}) - W_i(j\omega_{pc})XP_i(j\omega_{pc}) < -1/\underline{GM}. \tag{29}$$

2.4. LMIs for adjusting the phase margin

The LMIs presented in Sections 2.2 and 2.3 are mainly intended to shape the open-loop frequency response such that the closed-loop stability is achieved. However, they can also be used to adjust the GM through (21) and (29), and the speed of closed-loop system by appropriate choice of ω_{pc}. Hence, it is possible to design a stabilising controller with an adjustable GM and rise time simply by solving an LMI feasibility problem as described in previous sections.

The other characteristic of any feedback system which highly affects its time domain response is the PM. Clearly, for a given process model and controller structure it is not exactly known in advance whether a desired PM can be achieved or not. Hence, in order to arrive at a feedback system with a desired PM one should formulate the problem as a constrained optimization problem in X which firstly guarantees the closed-loop stability, and secondly, makes the PM of the resulted closed-loop system as close as possible to the desired value. Mathematically, it is equivalent to

$$\min_X \left\| W(j\omega_{gc})XP(j\omega_{gc}) - e^{j\varphi_m} \right\|, \tag{30}$$

where X satisfies the stability LMIs presented in Section 2.2 or 2.3, ω_{gc} is the desired gain crossover frequency, and $\varphi_m = \pi + PM$ is the desired value for open-loop phase at ω_{gc} (PM is the desired value for PM). According to the Schur complement lemma the minimization problem in (30) is equivalent to the generalized eigenvalue problem (GEVP):

$$\text{minimize} \quad \gamma, \tag{31}$$

subject to

$$\begin{pmatrix} 0 & e^{j\varphi_m} - W(j\omega_{gc})XP(j\omega_{gc}) \\ \left(e^{j\varphi_m} - W(j\omega_{gc})XP(j\omega_{gc})\right)^{\text{H}} & 0 \end{pmatrix} < \gamma I. \tag{32}$$

The only problem with (32) is that the matrix in it is complex while trivial LMI solvers accept only real matrices. In order to remove this difficulty we use the theorem [31], ch. 12 which states that for any Hermitian matrix $Q = Q_R + jQ_I = Q^{\text{H}}$, where Q_R and Q_I are real matrices, we have $Q < 0$ if and only if:

$$\begin{pmatrix} Q_R & Q_I \\ -Q_I & Q_R \end{pmatrix} < 0. \tag{33}$$

Applying this theorem to (32) leads to the following equivalent LMI:

$$\begin{pmatrix} 0 & \cos\varphi_m - W_rXP_r + W_iXP_i & 0 & \sin\varphi_m - W_rXP_i - W_iXP_r \\ \star & 0 & W_rXP_i + W_iXP_r - \sin\varphi_m & 0 \\ \star & \star & 0 & \cos\varphi_m - W_rXP_r + W_iXP_i \\ \star & \star & \star & 0 \end{pmatrix} < \gamma I. \tag{34}$$

(Since the matrix in (34) is symmetric, only the entries above the main diagonal are represented and the other entries are shown by $\star$ sign.) To sum up, in order to arrive at a stable closed-loop system with the desired PM, the GEVP (31) subject to the regular stability constraints of Section 2.2 or 2.3, and the linear fractional constraint (34) must be solved.

2.5. LMIs for shaping the phase of $L(j\omega)$

The other possible useful objective is to set only the phase of open-loop system at the given frequency ω_{ph} as close as possible to $\pi + \theta$ where $0 < \theta < \pi/2$ is the desired angle. For example, by choosing $\theta = PM$, where PM is the desired PM, and ω_{ph} a frequency rather close to ω_{gc} one can make the phase plot of open-loop frequency response versus frequency almost flat at frequencies around ω_{gc}. This flatness leads to a closed-loop system with iso-damped step response at the presence of uncertainties in the gain of process [3,32]. Note that in this manner the open-loop frequency response will be similar to the Bode's ideal transfer function in a certain frequency range around ω_{gc}.

The phase of open-loop system at $\omega = \omega_{ph}$ is equal to $\pi + \theta$ $(0 < \theta < \pi/2)$ if and only if the equation:

$$\tan\theta = \frac{\text{Im}\{W(j\omega_{ph})XP(j\omega_{ph})\}}{\text{Re}\{W(j\omega_{ph})XP(j\omega_{ph})\}}, \tag{35}$$

or equivalently,

$$F(X) \triangleq \left[W_i(j\omega_{ph})XP_r(j\omega_{ph}) + W_r(j\omega_{ph})XP_i(j\omega_{ph}) \right] \\ - \left[W_r(j\omega_{ph})XP_r(j\omega_{ph}) - W_i(j\omega_{ph})XP_i(j\omega_{ph}) \right]\tan\theta = 0, \tag{36}$$

holds at this frequency. Clearly, X can be considered as a very good approximate solution for (36) if it satisfies the inequalities $-\gamma < F(X) < \gamma$ for a very small positive real γ. Hence, X can be safely regarded as a solution for (36) if solving the GEVP: minimize γ subject to the linear fractional constraints:

$$\left[W_i(j\omega_{ph})XP_r(j\omega_{ph}) + W_r(j\omega_{ph})XP_i(j\omega_{ph}) \right] \\ - \left[W_r(j\omega_{ph})XP_r(j\omega_{ph}) - W_i(j\omega_{ph})XP_i(j\omega_{ph}) \right]\tan\theta < \gamma, \tag{37}$$

and

$$-\left[W_i(j\omega_{ph})XP_r(j\omega_{ph}) + W_r(j\omega_{ph})XP_i(j\omega_{ph}) \right] \\ + \left[W_r(j\omega_{ph})XP_r(j\omega_{ph}) - W_i(j\omega_{ph})XP_i(j\omega_{ph}) \right]\tan\theta < \gamma, \tag{38}$$

results in a γ very close to zero.

2.6. LMIs for shaping the amplitude of $L(j\omega)$

Suppose that at a certain frequency like ω_0 we want to have $|L(j\omega_0)| < \alpha$, or equivalently

$$|W(j\omega_0)XP(j\omega_0)| < \alpha, \tag{39}$$

for some positive real α. Eq. (39) yields

$$W(j\omega_0)XP(j\omega_0)P^{\text{H}}(j\omega_0)X^{\text{T}}W^{\text{H}}(j\omega_0) < \alpha^2, \tag{40}$$

or equivalently,

$$-\alpha^2 - W(j\omega_0)X\left\{ -\left|P(j\omega_0)\right|^2 \right\}X^{\text{T}}W^{\text{H}}(j\omega_0) < 0. \tag{41}$$

Inequality (41) is nonlinear in X but using Schur complement lemma it can be written as

$$\begin{pmatrix} -\alpha^2 & W(j\omega_0)X \\ X^{\mathrm{T}}W^{\mathrm{H}}(j\omega_0) & -\left|P(j\omega_0)\right|^{-2} \end{pmatrix} < 0, \tag{42}$$

which is linear in X. Following an approach similar to the one presented in Section 2.4 it can be easily verified that the complex inequality (42) is equivalent to the following real one:

$$\begin{pmatrix} -\alpha^2 & W_R(j\omega_0)X & 0 & W_I(j\omega_0)X \\ \star & -\left|P(j\omega_0)\right|^{-2} & -X^{\mathrm{T}}W_I^{\mathrm{T}}(j\omega_0) & 0 \\ \star & \star & -\alpha^2 & W_R(j\omega_0)X \\ \star & \star & \star & -\left|P(j\omega_0)\right|^{-2} \end{pmatrix} < 0. \tag{43}$$

2.7. Higher order and time-delayed processes with one unstable pole

The method proposed in this section can be used for tuning the parameters of any controller of the form $C(s) = W(s)X$ when $P(s)$ has exactly one unstable pole. This method is especially useful when the process has time delay and/or is of high order such that encirclement of the Nyquist plot around the origin is unavoidable. Clearly, assuming that $P(s)$ has exactly one unstable pole, the closed-loop system is stable if the Nyquist plot of $L(j\omega)$ remains in the hatched region in Fig. 4 for all $\omega \geq 0$, where $L_i(j\omega)$ and $L_r(j\omega)$ stand for $\mathrm{Im}\{L(j\omega)\}$ and $\mathrm{Re}\{L(j\omega)\}$, respectively. Note that although this condition is of sufficient type, it is not tight and covers a wide variety of situations. The border of the hatched region in Fig. 4 is identified by three lines which are plotted such that firstly the origin belongs to the hatched region (i.e., $b_3 > 0$) and secondly the point -1 stays out of it. Moreover, we must have $0 < a_3 < a_1$ to make sure that it is impossible to draw a simple closed contour in the hatched region which encircles -1. As it can be observed in Fig. 4 one can adjust the bounds of $\underline{GM}$ and $\overline{GM}$ simply by appropriate choice of a_1, b_1, a_3, and b_3.

In order to tune the parameters of the controller first assign suitable values to a_i and b_i ($i = 1, 2, 3$). Note that depending on the process model, considering a big empty region around -1 may make the problem infeasible. Denote the frequency at which the Nyquist plot intersects the negative real axis for the first time as ω_{gml}. The speed of closed-loop system response can be adjusted indirectly by changing ω_{gml} such that larger ω_{gml} leads to a faster response and vice versa. Moreover, in Fig. 4 the stability properties and overshoots of the closed-loop step response can be determined indirectly by adjusting the size of the empty region around -1 (through a_i and b_i, $i = 1, 2, 3$) where a larger empty region leads to a more stable closed-loop system. According to the previous discussions, in order to keep the Nyquist plot of $L(j\omega)$ in the hatched region for $\omega \geq 0$ the following LMIs in X must be satisfied simultaneously:
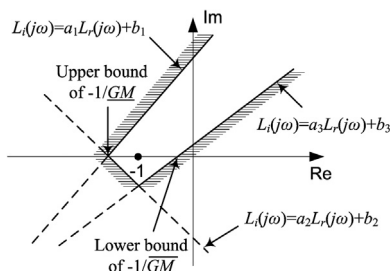

Fig. 4. The hatched region shows the location of the Nyquist plot of $L(j\omega)$ to achieve closed-loop stability when $P(s)$ has exactly one unstable pole.

$$W_i(j\omega_k)XP_r(j\omega_k) + W_r(j\omega_k)XP_i(j\omega_k) > a_1\big(W_r(j\omega_k)XP_r(j\omega_k)$$
$$-W_i(j\omega_k)XP_i(j\omega_k)\big) + b_1, \quad 0 \leq \omega_k < \omega_1, \tag{44}$$

$$W_i(j\omega_k)XP_r(j\omega_k) + W_r(j\omega_k)XP_i(j\omega_k) < a_2\big(W_r(j\omega_k)XP_r(j\omega_k)$$
$$-W_i(j\omega_k)XP_i(j\omega_k)\big) + b_2, \quad \omega_1 < \omega_k < \omega_2, \tag{45}$$

$$W_i(j\omega_k)XP_r(j\omega_k) + W_r(j\omega_k)XP_i(j\omega_k) < a_3\big(W_r(j\omega_k)XP_r(j\omega_k)$$
$$-W_i(j\omega_k)XP_i(j\omega_k)\big) + b_3, \quad \omega_2 < \omega_k < \infty, \tag{46}$$

$$-\epsilon < W_i(j\omega_{gml})XP_r(j\omega_{gml}) + W_r(j\omega_{gml})XP_i(j\omega_{gml}) < \epsilon, \tag{47}$$

$$W_r(j\omega_{gml})XP_r(j\omega_{gml}) - W_i(j\omega_{gml})XP_i(j\omega_{gml}) < -1/\underline{GM}, \tag{48}$$

where ω_k are the frequency samples chosen from the frequency interval under consideration, ϵ is a small positive real constant and $\underline{GM}$ is the desired value for GM. Inequalities (44)–(46) are used to define the three half-planes in Fig. 4, and (47) and (48) are used to make sure that the Nyquist plot intersects the negative real axis at the desired position and frequency. ω_1 and ω_2 in (44)–(46) are the frequencies determined by designer which specify the maximum frequencies for which the Nyquist plot must remain in the corresponding half plane.

3. Illustrative examples

Four numerical examples are presented in this section. In all of the following examples the unit step response of the closed-loop system is calculated by taking the numerical inverse Laplace transform from $CP/(1 + CP)s$ by using the Matlab function invlap. m, which can be easily accessed by a search on internet. All of the LMIs are solved by using the LMI solver of Matlab R2014b. In Examples 1–3 the parameters of the FOPID controller are calculated by solving a constrained optimization problem using the genetic algorithm (GA) toolbox of Matlab R2014b where the optimization is run 100 times using the default values of parameters (except the population size which is set to 200) and the best result is reported. During this optimization the order of fractional integrator and differentiator is limited to the range [0, 2]. M_s, P. O., t_r and t_s stand for the maximum sensitivity, percent of overshoot, rise time, and settling time (5% criterion), respectively.

Example 1. The transfer function of a non-laminated electro-magnetic suspension system can be expressed as [33]:

$$P(s) = \frac{K}{s^{2.5} + s^2 - c}, \tag{49}$$

where K and c are positive real constants. It can be shown that for any positive real c this transfer function has exactly one unstable pole and therefore the LMIs proposed in Section 2.3 for closed-loop stability can be applied. In the following, without any loss of generality, we assume that $K = c = 1$. The aim of this example is to tune the parameters of the controllers:

$$C_{PID}(s) = k_p + k_i\frac{1}{s} + k_d s, \tag{50}$$

$$C_{MFOPID}(s) = k_p + k_i\frac{1}{s} + k_{d1}s + k_{d2}s^{0.5}, \tag{51}$$

ARTICLE IN PRESS

6   *F. Merrikh-Bayat / ISA Transactions ▪ (▪▪▪▪) ▪▪▪–▪▪▪*

$$C_{TID}(s) = k_t \frac{1}{s^{0.5}} + k_i \frac{1}{s} + k_d s, \tag{52}$$

such that the control objectives: closed-loop stability with $1/\underline{GM} = 20$ dB, phase crossover frequency $\omega_{pc} = 1$ rad/s, gain crossover frequency $\omega_{gc} = 5$ rad/s, phase margin $PM = 65°$, and open-loop phase at $\omega_{ph} = 3$ rad/s equal to $65°$ are met. The required LMIs are listed below:

- for closed-loop stability use (25) for $\omega = 10^{-3}, 10^{-2}, 10^{-1}$ rad/s (all smaller than $\omega_{pc} = 1$ rad/s), (29) with $1/\underline{GM} = 20$ dB, (27) with $\epsilon = 0.01$, and (28) for $\omega = 10, 10^2$ rad/s (all larger than $\omega_{pc} = 1$ rad/s),
- to adjust the PM solve the GEVP defined through (31) and (34) where W_r, W_i, P_r, and P_i are all evaluated at $\omega_{gc} = 5$ rad/s and $\varphi_m = 180° + PM = 245°$,
- to adjust the open-loop phase at $\omega_{ph} = 3$ rad/s to $180° + \theta = 180° + PM = 245°$ solve the GEVP defined through (31), (37), and (38).

To sum up, in order to reach all of the control objectives simultaneously, a GEVP consists of (31), (34), (37), (38), (25), (27), (28), and (29) evaluated at the given samples of ω must be solved. Note that the GEVP solver of Matlab expects that the linear fractional constraints in γ, i.e. (34), (37), and (38), are entered last during programming. After solving these LMIs we have $\left(k_p, k_i, k_d\right) = (27.0775, 0.1037, 7.1784)$ for PID,

$\left(k_p, k_i, k_{d1}, k_{d2}\right) = (59.3221, -2.4927 \times 10^{-5}, 39.2907, -45.5964)$

for MFOPID, and $\left(k_t, k_i, k_d\right) = (38.3413, -0.8071, 33.3863)$ for TID. An FOPID is also tuned using GA such that the same control objectives are met. For this purpose the cost function to be minimized is mathematically defined as

$$J = \left| L(j\omega_{gc}) - e^{-j(180° - PM)} \right| + \left| \sin\left(\angle L(j\omega_{ph}) - (PM - 180°) \right) \right|, \tag{53}$$

subject to the inequality constraints (25), (28), and (29) (for appropriate sample values of ω and the $\underline{GM}$ as described above), and the equality constraint (27). Parameters of the resulted optimal FOPID are $\left(k_p, k_i, k_d, \lambda, \mu\right) = (28.6428, 24.2442, 15.2539, 0.0462, 1.2666)$.

The Bode plots of the shaped open-loop systems are shown in Fig. 5. In this figure the frequencies used in the formulation of LMIs are shown by triangles and the important data points are shown by diamonds. As it can be observed in Fig. 5, at $\omega_{pc} = 1$ rad/s the phase angle of all open-loop systems is approximately equal to $180°$ and their magnitude is larger than 20 dB. This result was expected as a direct consequent of stability constraints. It was also expected that at $\omega_{ph} = 3$ rad/s and $\omega_{gc} = 5$ rad/s the phase angle becomes as close as possible to $245°$, and simultaneously, at the later frequency the magnitude becomes as close as possible to 0 dB. Fig. 5 shows that at $\omega_{gc} = 5$ rad/s all of the controllers approximately satisfy the desired magnitude condition but only the MFOPID fairly satisfies the required phase angle conditions at $\omega = 3$ rad/s and $\omega = 5$ rad/s. That is because the MFOPID controller has two derivative terms which make it capable of producing more phase lead.

The order of fractional differentiator in (51) was set to 0.5 in advance. In order to show that the results are not so sensitive to the special value assigned to this parameter, the design procedure is repeated with $\mu = 0.4, 0.6, 0.7$ as well and the results are shown in Fig. 5. According to this figure, the most important thing is the existence of the fractional-order derivative operator in (51), but not its degree.
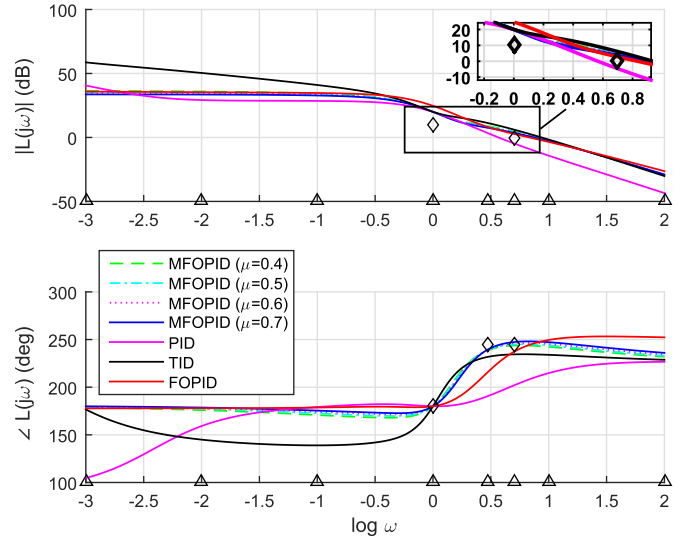

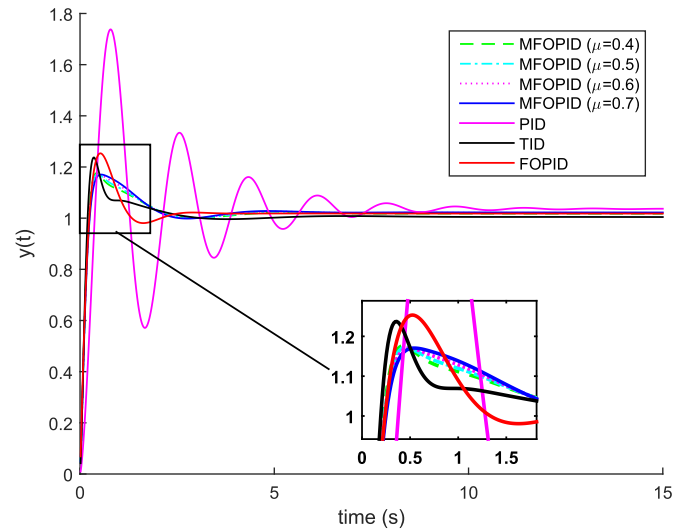**Fig. 5.** Bode plots of $L(j\omega)$, corresponding to Example 1.

Fig. 6. Unit step responses of the closed-loop system, corresponding to Example 1.

The closed-loop unit step responses and the corresponding control efforts are shown in Figs. 6 and 7, respectively. As it is expected, the MFOPID leads to the response with the smallest overshoot. Fig. 6 also shows that if we repeat the simulation with other values for the order of fractional differentiator in (51), the final results are not affected so much. Note also that the results obtained in this example are not so sensitive to the sample frequencies used to derive the required LMIs for closed-loop stability. Table 1 summarizes the results.

Example 2. Consider a FOS with one unstable pole as the following:

$$P(s) = \frac{2}{\left(1 - 4s^{1/2}\right)\left(1 + 7s^{2/3}\right)(1 + 5s)}. \tag{54}$$

The aim is to tune the controllers:

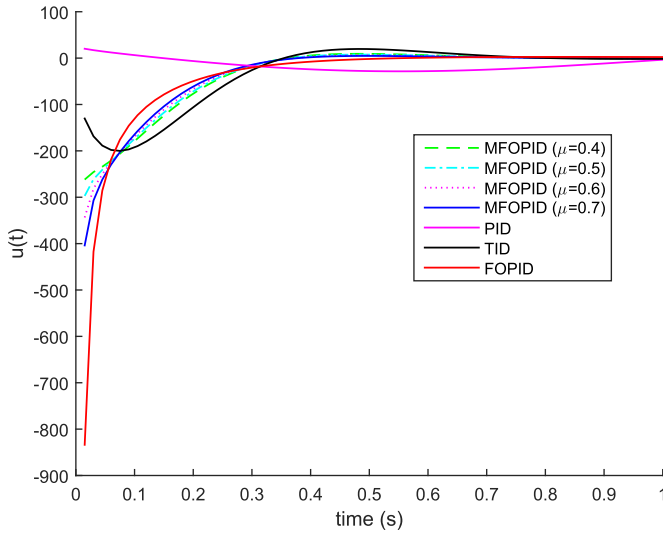$$C_{PID}(s) = k_p + k_i \frac{1}{s} + k_d \frac{s}{1 + 10^{-4}s}, \tag{55}$$

Fig. 7. Control efforts, corresponding to Example 1.

Fig. 8. Bode plots of $L(j\omega)$, corresponding to Example 2.

Table 1
Summary of the results for Example 1.

	M_s	P. O.(%)	$t_r(s)$	$t_s(s)$
MFOPID ($\mu = 0.4$)	1.15	18	0.23	1.76
MFOPID ($\mu = 0.5$)	1.14	17	0.23	1.76
MFOPID ($\mu = 0.6$)	1.12	17	0.24	1.76
MFOPID ($\mu = 0.7$)	1.10	17	0.25	1.76
PID	3.80	74	0.38	8.15
TID	1.25	24	0.20	1.55
FOPID	1.05	25	0.24	1.13

$$C_{MFOPID}(s) = k_p + k_i\frac{1}{s} + k_{d1}\frac{s}{1 + 10^{-4}s} + k_{d2}\frac{s^{0.8}}{1 + 10^{-4}s}, \tag{56}$$

$$C_{TID}(s) = k_t\frac{1}{s^{0.5}} + k_i\frac{1}{s} + k_d\frac{s}{1 + 10^{-4}s}, \tag{57}$$

such that the control objectives: closed-loop stability with $1/\underline{GM} = 3$, phase crossover frequency $\omega_{pc} = 100$ rad/s, gain crossover frequency $\omega_{gc} = 500$ rad/s, phase margin $PM = 70°$, and open-loop phase at $\omega_{ph} = 300$ rad/s equal to $70°$ are achieved. The required LMIs to reach the above design specifications are as the following:

- for closed-loop stability use (25) for $\omega = 0.1, 10, 50$ rad/s (all smaller than $\omega_{pc} = 100$ rad/s), (29) with $1/\underline{GM} = 3$, (27) with $\epsilon = 0.01$, and (28) with $\omega = 2 \times 10^3, 10^4$ rad/s (all larger than $\omega_{pc} = 100$ rad/s).
- to adjust the PM to $70°$ and the phase at $\omega_{ph} = 300$ rad/s to $70°$ solve the GEVP defined through (31), (34), (37), and (38) where W_r, W_i, P_r, and P_i are all evaluated at $\omega_{gc} = 500$ rad/s and $\varphi_m = 180° + PM = 250°$.

After solving the above GEVP for each controller separately, the following results are obtained:

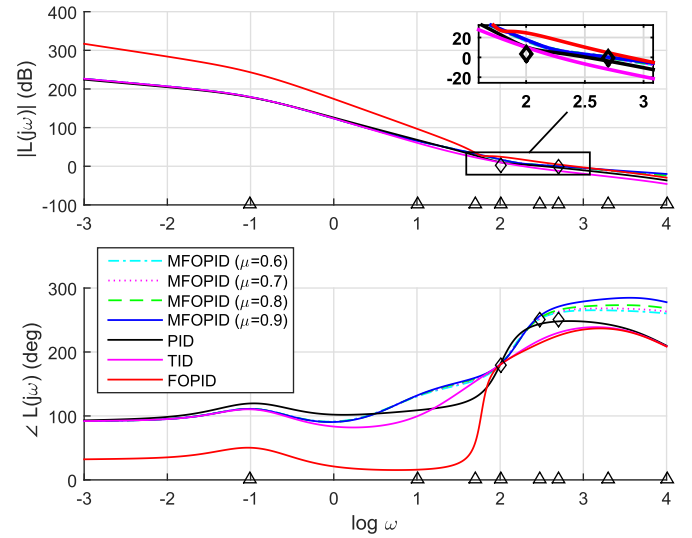$$C_{PID}(s) = 10^7\left(-0.4576 - \frac{9.9827}{s} - \frac{0.00238s}{1 + 10^{-4}s}\right), \tag{58}$$

$$C_{MFOPID}(s)$$
$$= 10^7\left(-1.7412 - \frac{9.8396}{s} - \frac{0.0237s}{1 + 10^{-4}s} + \frac{0.0519\,s^{0.8}}{1 + 10^{-4}s}\right), \tag{59}$$

$$C_{TID}(s) = 10^7\left(-\frac{6.6811}{s^{0.5}} - \frac{7.4362}{s} - \frac{0.0068s}{1 + 10^{-4}s}\right). \tag{60}$$

Using the procedure similar to Example 1 the following FOPID controller is also designed:

$$C_{FOPID}(s) = 10^7\left(-3.8130 - \frac{3.3840 \times 10^3}{s^{1.6642}} - \frac{1.4805 \times 10^{-2}s}{1 + 10^{-4}s}\right). \tag{61}$$

Bode plots of the resulted open-loop systems are shown in Fig. 8. The closed-loop unit step responses and the corresponding control efforts are shown in Figs. 9(a) and (b), respectively. In this example the PID controller cannot provide the required phase lead, and consequently, the corresponding overshoots in the step
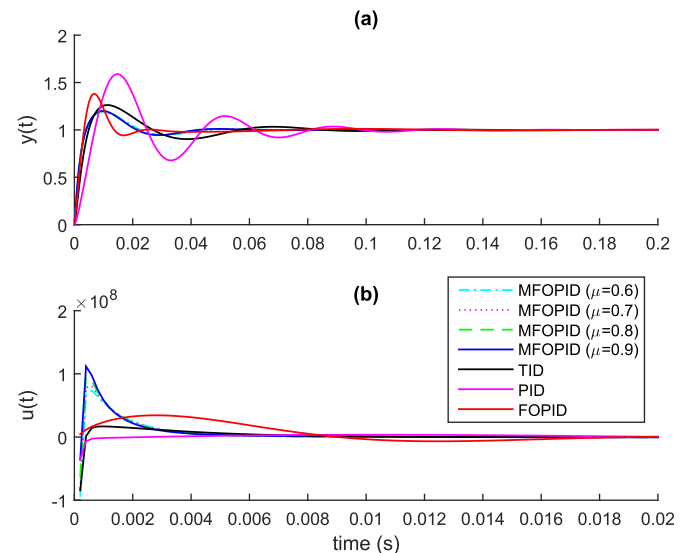

Fig. 9. (a) unit step responses of the closed-loop system, (b) control efforts, corresponding to Example 2.

Table 2
Summary of the results for Example 2.

	M_s	P. O.(%)	t_r(ms)	t_s(ms)
MFOPID ($\mu = 0.6$)	1.01	20	4.0	32.0
MFOPID ($\mu = 0.7$)	1.01	20	4.0	32.0
MFOPID ($\mu = 0.8$)	1.00	20	4.0	32.0
MFOPID ($\mu = 0.9$)	1.00	20	4.0	32.0
PID	2.42	59	7.0	75.9
TID	1.09	26	5.0	49.3
FOPID	1.21	38	3.2	18.6

response are much larger than FOPID, MFOPID, and TID. In Figs. 8 and 9 the results are presented for various values of μ. As it is observed, the results exhibit a low sensitivity to the variations of this parameter. It means that although the order of the fractional differentiator of MFOPID is fixed beforehand, it does not highly affect the final results. Table 2 summarizes the results of this example.

Example 3. In this example the transfer function of process is similar to Example 1 with the difference that it also has a time-delay as the following:

$$P(s) = \frac{e^{-0.05s}}{s^{2.5} + s^2 - 1}. \tag{62}$$

Stability of a closed-loop system consisting of a process with transfer function (62) and a PD^μ controller is studied in [34]. We use the method proposed in Section 2.7 to tune the parameters of the controllers given in (50)–(52) (MFOPID with $\mu = 0.6, 0.7, 0.8, 0.9$ is studied in the following). Assuming $a_1 = b_1 = 1$, $a_2 = b_2 = -0.3$, $a_3 = 0.3$, $b_3 = 0.2$, solving the LMI feasibility problem consisting of (44) (for $\omega = 10^{-3}, 10^{-2}, 10^{-1}$ rad/s), (45) (for $\omega = 4, 8, 16$ rad/s), (46) (for $\omega = 30, 60, 90, …, 510$ rad/s), (47) (for $\omega_{gml} = 1$ rad/s and $\epsilon = 0.05$), and (48) (for $\underline{GM} = 0.1$) results in the following controllers:

$$C_{PID}(s) = 32.2548 + \frac{42.0855}{s} + 52.2569s, \tag{63}$$

$$C_{MFOPID}(s) = 50.0318 - \frac{0.0097}{s} + 79.5567s - 74.7289s^{0.8}, \tag{64}$$

$$C_{TID}(s) = \frac{44.2564}{s^{0.5}} + \frac{9.6717}{s} + 50.8376s. \tag{65}$$

Note that the delay term in (62) generates about $-\pi/2$ rad phase lag for every 30 rad/s increasing of the frequency. Hence, in (46) the frequency samples are considered with the steps of 30 rad/s to make sure that there is at least one sample of open-loop frequency response at each quarter plane.

An FOPID controller is also designed using GA. For this purpose the main cost function to be minimized is considered as $J = \left| \text{Im}\{L(j\omega_{gml})\} \right|$ subject to the inequality constraints as mentioned in the paragraph above (63) (except (47) which is included in cost function). The resulted FOPID is

$$C_{FOPID}(s) = 77.5367 + \frac{29.5014}{s^{0.0028}} + 32.3440s^{1.1675}. \tag{66}$$

Fig. 10 shows the resulted Nuquist plots. The picture zoomed around the origin shows that the Nyquist plot corresponding to MFOPID has a smaller distance from the origin at the second point of intersection with the negative real axis. More precisely, in the picture zoomed around the origin the intersection point of Nyquist
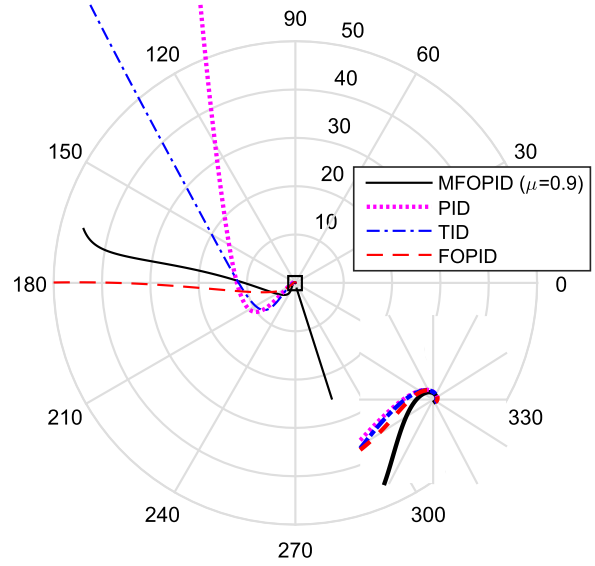

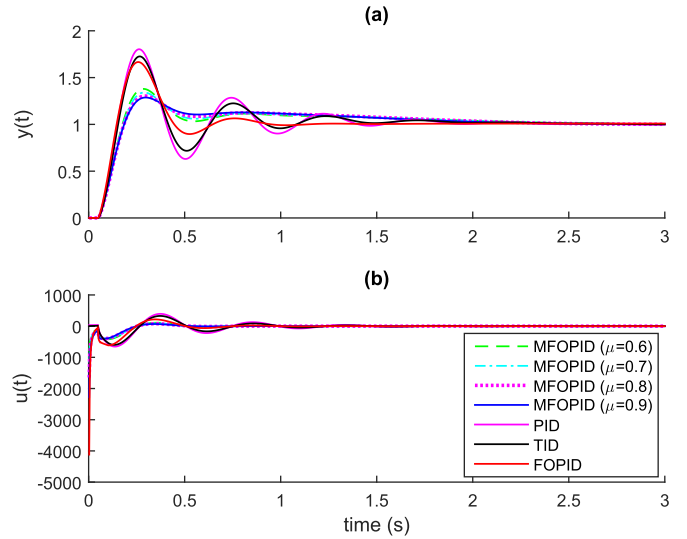**Fig. 10.** Nyquist plots of $L(j\omega)$, corresponding to Example 3.

Fig. 11. (a) unit step responses of the closed-loop system, (b) control efforts, corresponding to Example 3.

plots with the negative real axis is equal to -0.5833, -0.3684, -0.5421, -0.4490 for PID, MFOPID, TID, and FOPID respectively. It means that MFOPID leads to a more stable closed-loop system.

Figs. 11(a) and (b) show the corresponding closed-loop unit step responses and control efforts, respectively. In order to show that the results are not so sensitive to the value assigned to μ, in Fig. 11 the results are presented for various values of μ. This figure clearly shows that adding a fractional-order differentiator to the classical PID can considerably improve the transient response and stability properties of the closed-loop system at the cost of a slightly slower convergence of response to its final value. Table 3 summarizes the results of this example.

Example 4. A process with transfer function $P(s) = 3.13e^{-50s}/(433.33s + 1)$ is considered in [32] and a FOPID is designed through nonlinear optimization techniques such that the resulted closed-loop system simultaneously satisfies the constraints: $\omega_{gc} = 0.008$ rad/s, $PM = 60°$,

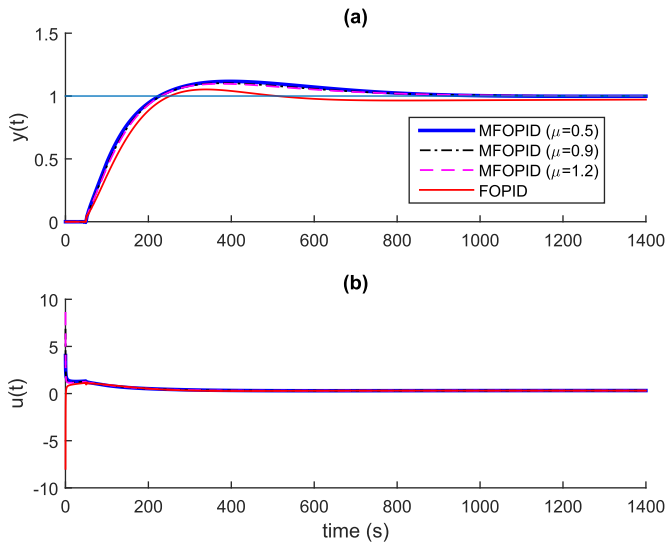$$|S(j\omega)| < 0.1, \quad \omega \le 0.05\omega_{gc}, \tag{67}$$

Table 3
Summary of the results for Example 3.

	M_s	P. O.(%)	t_r(s)	t_s(s)
MFOPID ($\mu = 0.6$)	2.02	38	0.18	1.83
MFOPID ($\mu = 0.7$)	1.92	34	0.18	1.83
MFOPID ($\mu = 0.8$)	1.83	30	0.19	1.81
MFOPID ($\mu = 0.9$)	1.78	29	0.19	1.72
PID	4.04	80	0.15	1.72
TID	3.48	73	0.15	1.36
FOPID	2.60	67	0.14	0.83

Table 4
Summary of the results for Example 4.

	M_s	P. O.(%)	t_r(s)	t_s(s)
MFOPID ($\mu = 0.5$)	1.41	9.6	248.9	712.1
MFOPID ($\mu = 0.9$)	1.38	5.8	259.4	524.9
MFOPID ($\mu = 1.2$)	1.38	4.7	262.2	223.5
FOPID	1.26	5.2	252.4	361.0

Fig. 12. (a) unit step responses of the closed-loop system, (b) control efforts, corresponding to Example 4.

$$|T(j\omega)| < 0.1, \quad \omega > 50\omega_{gc}, \tag{68}$$

$$\left. \frac{d\{\arg L(j\omega)\}}{d\omega} \right|_{\omega = \omega_{gc}} = 0, \tag{69}$$

where $S \triangleq 1/(1 + CP)$ and $T \triangleq CP/(1 + CP)$. The resulted FOPID is $C_{FOPID}(s) = 0.8617\left(1 + 1/59.9987s^{0.7419} + 7.0088s^{1.1669}\right)$ [32].

Now we derive the required LMIs for tuning the proposed MFOPID such that the above constraints are satisfied. The problem is formulated as a GEVP consisting of (31) and (34) (assuming $\varphi_m = 180 + 60 = 240°$) subject to the constraints caused by (67)–(69). In order to satisfy (67) it is sufficient to have $|L(j\omega)| > 11$ for $\omega \le 0.05\omega_{gc}$ which leads to a non-convex inequality in X. Hence, we use the inequality $\text{Im}\{L(j0.05\omega_{gc})\} < -11$ instead of that in practice. Note that according to the discussions of Section 2.2 it is expected that the Nyquist plot of $L(j\omega)$ lies in the lower half plane at low frequencies; hence, $|L(j\omega)| > 11$ can safely be interpreted as $\text{Im}\{L(j\omega)\} < -11$. In order to satisfy (68) it is sufficient to have $|L(j\omega)| < 1/11$ for $\omega > 50\omega_{gc}$ which is convex in X and can be formulated using (43) assuming $\alpha = 1/11$ and $\omega_0 = 50\omega_{gc}$. Finally, (69) can be addressed using (37) and (38) assuming $\theta = PM$ and $\omega_{ph} = 10\omega_{gc}$ (to keep the open-loop phase as flat as possible in the frequency range $[\omega_{gc}, 10\omega_{gc}]$). No LIMs for closed-loop stability are applied to this problem since it was observed that using only the above-mentioned LMIs leads to a stable closed-loop system.

The resulted MFOPID assuming $\mu = 0.5$ is $C_{MFOPID}(s) = 0.9293 + 0.0047/s + 0.8828s + 2.0606s^{0.5}$. Unit step responses of the closed-loop system and the corresponding control efforts are shown in

Figs. 12(a) and (b), respectively for $\mu = 0.5, 0.9, 1.2$. Similar to the previous examples it is observed that the MFOPID exhibits a very low sensitivity to the value of μ. Note that the step response of the FOPID-controlled system converges to its final value very slowly since the order of its fractional integrator is smaller than unity. Table 4 summarizes the results of this example.

4. Conclusion

In this paper we introduced the MFOPID controller whose transfer function is equal to the linear combination of fractional powers of s such that each power is equal to a distinct real constant. In the numerical simulations we mainly focused on a special form of MFOPID, the four-variable MFOPID, whose transfer function is similar to a traditional PID with an extra fractional differentiator of fixed order. Similar to PID and TID, the MFOPID is linear in its parameters and as it was shown in this paper these parameters can be tuned using LMIs.

The simulations revealed two main facts about the four-variable MFOPID. First, although the order of fractional differentiator is considered fixed in advance, the final results exhibit a low sensitivity to the value assigned to it. Hence, it is expected that the suitable value of this parameter can be determined by a simple trial and error. In fact it is expected that initial choices like 0.5 or 0.8 for μ lead to satisfactory results in dealing with a wide variety of problems. The second observation is that a four-variable MFOPID can, more or less, be as efficient as a FOPID. However, MFOPID has the advantage of being tunable using LMIs and convex optimization techniques.

References

[1] Podlubny I. Fractional-order systems and $PI^\lambda D^\mu$-controllers. IEEE Trans Autom Control 1999;44:208–14.
[2] Valerio D. Introduction to single-input, single-output fractional control. IET Control Theory A 2011;5:1033–57.
[3] Monje CA, Vinagre BM, Feliu V, Chen YQ. Tuning and auto-tuning of fractional order controllers for industry applications. Control Eng Pract 2008;16:798–812.
[4] Li HS, Luo Y, Chen YQ. A fractional order proportional and derivative (FOPD) motion controller: tuning rule and experiments. IEEE Trans Control Syst Technol 2010;18:516–20.
[5] Chao H, Luo Y, Di L, Chen YQ. Roll-channel fractional order controller design for a small fixed-wing unmanned aerial vehicle. Control Eng Pract Vol 2010;18:761–72.
[6] Zhang M, Lin X, Yin W. An improved tuning method of fractional order proportional differentiation (FOPD) controller for the path tracking control of tractors. Biosyst Eng 2013;116:478–86.
[7] Beschi M, Padula F, Visioli A. Fractional robust PID control of a solar furnace. Control Eng Pract 2016;56:190–9.
[8] Podlubny I, Petras I, Vinagre BM, O'Leary P, Dorcak L. Analogue realizations of fractional-order controllers. Nonlinear Dyn 2002;29:281–96.
[9] Charef A. Analogue realisation of fractional-order integrator, differentiator and fractional $PI^\lambda D^\mu$ controller. IEE Proc- Control Theory Appl 2006;153:714–20.
[10] Barbosa RS, Tenreiro Machado JA. Implementation of discrete-time fractional-order controllers based on LS approximations. Acta Polytech Hung 2006;3:5–22.
[11] Merrikh-Bayat F, Mirebrahimi N, Khalili MR. Discrete-time fractional-order PID controller: definition, tuning, digital realization and some applications. Int J Control, Autom Syst 2015;13:81–90.
[12] Lurie BJ. Three-parameter tunable tilt-integral-derivative (TID) Controller. United States Patent; 1994.

[13] Xue D, Chen YQ. A comparative introduction of four fractional order controllers. Proceedings of the 4th World congress on intelligent control and automation, Shanghai, China; June 10–14, 2002, pp. 3228–3235.

[14] Luo Y, Chen YQ, Wang CY, Pi YG. Tuning fractional order proportional integral controllers for fractional order systems. J Process Control 2010;20:823–31.

[15] Barbosa RS, Tenreiro Machado JA, Ferreira IM. Tuning of PID controllers based on Bode's ideal transfer function. Nonlinear Dynam 2004;38:305–21.

[16] Vu TNL, Lee M. Analytical design of fractional-order proportional-integral controllers for time-delay processes. ISA Trans 2013;52:583–91.

[17] Merrikh-Bayat F. General rules for optimal tuning the $PI^{\lambda}D^{\mu}$ controllers with application to first-order plus time delay processes. Can J Chem Eng 2012;90:1400–10.

[18] Padula F, Visioli A. Optimal tuning rules for proportional-integral-derivative and fractional-order proportional-integral-derivative controllers for integral and unstable processes. IET Control Theory A 2012;6:776–86.

[19] Chen YQ, Bhaskaran T, Xue D. Practical tuning rule development for fractional order proportional and integral controllers. J Comput Nonlinear Dyn- T ASME 2008;3:021403.

[20] El-Khazali R, Fractional-order PI. Fractional-order $PI^{\lambda}D^{\mu}$ controller design. Comput Math Appl 2013;66:639–46.

[21] Merrikh-Bayat F, Karimi-Ghartemani M. Method for designing $PI^{\lambda}D^{\mu}$ stabilisers for minimum-phase fractional-order systems. IET Control Theory A 2010;4:61–70.

[22] Biswas A, Das S, Abraham A, Dasgupta S. Design of fractional-order $PI^{\lambda}D^{\mu}$ controllers with an improved differential evolution. Eng Appl Artif Intel 2009;22:343–50.

[23] Chen Z, Yuan X, Ji B, Wang P, Tian H. Design of a fractional order PID controller for hydraulic turbine regulating system using chaotic non-dominated sorting genetic algorithm II. Energ Convers Manag 2014;84:390–404.

[24] Lee CH, Chang FK. Fractional-order PID controller optimization via improved electromagnetism-like algorithm. Expert Syst Appl 2010;37:8871–8.

[25] Boyd S, Ghaoui LE, Feron E, Balakrishnan V. Linear matrix inequalities in system and control theory.Philadelphia, PA: SIAM; 1994.

[26] Sabatier J, Moze M, Farges C. LMI stability conditions for fractional order systems. Comput Math Appl 2010;59:1594–609.

[27] Adelipour S, Abooee A, Haeri M. LMI-based sufficient conditions for robust stability and stabilization of LTI-fractional-order systems subjected to interval and polytopic uncertainties. Trans Inst Meas Control 2015;5:1207–16.

[28] Farges C, Moze M, Sabatier J. Pseudo-state feedback stabilization of commensurate fractional order systems. Automatica, 46; 2010, 1730–1734.

[29] Fadiga L, Farges C, Sabatier J, Santugini K. H_{∞} output feedback control of commensurate fractional order systems. In: Proceedings of the 12th European control conference (ECC), Zurich, Switzerland; 2013, pp. 4538–4543.

[30] Liang S, Wei YH, Pan JW, Gao Q, Wang Y. Bounded real lemmas for fractional order systems. Int J Autom Comput 2015;12:192–8.

[31] Skogestad S, Postlethwaite I. Multivariable feedback control: analysis and design. 2nd ed.. NJ: John Wiley & Sons; 2005.

[32] Beschi M, Padula F, Visioli A. The generalised isodamping approach for robust fractional PID controllers design. International J Control http://dx.doi.org/10.1080/00207179.2015.1099076.

[33] Knospe CR, Zhu L. Performance limitations of non-laminated magnetic suspension systems. IEEE Trans Control Syst Tecjnol 2011;19:327–36.

[34] Özbay H, Bonnet C, Fioravanti AR. PID controller design for fractional-order systems with time delays. Syst Control Lett 2012;61:18–23.